Essay

Not peer-reviewed version

Multi-Field Coupling Analysis of Resistance Spot Welding of SUS301L/Q235B Dissimilar Steel Based on Nickel Intermediate Layer

Xiaoqi Zhang *, Jinhao Li, Chengxian Yuan, Long Wang, Zhongliang Gao

Posted Date: 12 March 2026

doi: 10.20944/preprints202603.1017.v1

Keywords: dissimilar steel linkage resistance spot welding; nickel intermediate layer multi-field coupling simulation

 doi:10.20944/preprints202603.1017.v1

Essay

Multi-Field Coupling Analysis of Resistance Spot Welding of SUS301L/Q235B Dissimilar Steel Based on Nickel Intermediate Layer

Xiaoqi Zhang [1,*], Jinhao Li [1], Chengxian Yuan [1], Long Wang [1] and Zhongliang Gao [2]

[1] College of Engineering, Changchun Normal University, Changchun 130032, Jilin

[2] Quality Assurance Department, CRRC Changchun Railway Vehicles Co., Ltd., Changchun 130062, Jilin

* Correspondence: zhangxq@ccsfu.edu.cn

Abstract

Resistance spot welding of dissimilar steels is a key Linkage process in the manufacturing of rail passenger car bodies. However, there are problems such as core deviation caused by material physical property differences in the welding of dissimilar steels (stainless steel/low-carbon steel). This study improves the weldability of stainless steel and low-carbon steel by adding a nickel intermediate layer between them. The results show that adding a nickel intermediate layer can Valid compensate for heat Loss, suppress the deviation of the weld nucleus, optimize the size of the weld nucleus, and improve the Stability of the welding quality.

Keywords: dissimilar steel linkage resistance spot welding; nickel intermediate layer multi-field coupling simulation

0. Introduction

In the manufacturing of lightweight rail passenger cars, to meet the requirements of material performance and economic benefits for the car body structure, SUS301L austenitic stainless steel and Q235B low-carbon steel are often used for dissimilar material Linkage [1,2]. SUS301L stainless steel is widely [3] used in thin-walled components due to its good formability and work hardening effect. However, when performing resistance spot welding, the two materials have differences in physical Attribute, especially in resistivity and thermal conductivity, which leads to an imbalance in the Distribution of current and heat during the welding process, and the weld core often devi [4]ates towards the side of the stainless steel with lower thermal conductivity. More importantly, under the effect of high-temperature welding thermal Recurrence, brittle Fe-Cr carbides and hard and brittle σ phases are prone to form at the interfaces of heterogeneous [5,6] materials. The formation of these brittle phases will significantly reduce the toughness of the joint and adversely affect [7,8] its fatigue life.

To regulate the interfacial reaction and thermodynamic behavior, the introduction of a nickel intermediate layer was studied to improve the weldability of dissimilar steels. Nickel has electrical and thermal properties between the two base materials, improving current Distribution and inhibiting the formation of harmful phases. Existing research has mostly focused on process experiments and lacks systematic quantitative analysis of the electric-thermal-force-metallurgical coupling process. Therefore, this paper intends to establish a multi-field coupling Numeric Value Model for resistance spot welding of SUS301L/Q235B dissimilar steel, with a focus on studying the regulation mechanism of the nickel interlayer on the thermal Recurrence, nucleation morphology, stress Evolution and interfacial phase transformation during the welding process.

 doi:10.20944/preprints202603.1017.v1

1. Trial Materials

The Trial was conducted using 2mm thick SUS301L stainless steel plates and Q235B low-carbon steel plates. The thicknesses of the nickel intermediate layer are 0.3mm and 1mm respectively. The spot welding process uses CuCrZr material conical electrodes with an electrode end face diameter of 8mm. The chemical composition of the sheet is shown in Table 1.

Table 1. Chemical Composition (mass Percentage) of Trial Plates and copper Electrodes.

Trial sheet	Mass Percentage							
	C	Si	Mn	P	S	Ni	Cr	N
SUS301L	0.024	0.37	1.12	0.026	0.002	7.53	17.71	0.11
Q235B	0.18	0.26	0.54	0.004	0.005	--	--	--
CU electrode	--	0.05	--	0.01	--	--	0.8	--
Ni	0.02	0.35	0.35	--	0.01	99	--	--

2. Finite Element Model

2.1. Finite Element Modeling

Based on the strong Non-Linearity and multi-physical field coupling characteristics of the resistance spot welding process, in order to deeply study the influence of the nickel intermediate layer on the Linkage mechanism of SUS301L stainless steel and Q235B low-carbon steel dissimilar materials, this study establishes a comprehensive consideration of heat. The finite element analysis Model of the multi-field coupling effect of electricity and force is shown in Figure 1.

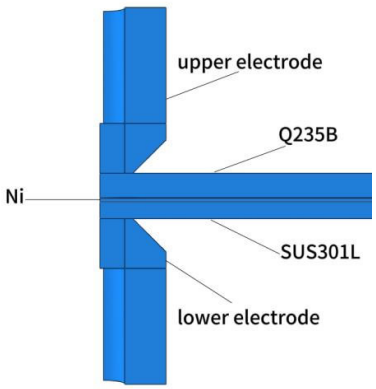

Figure 1. Schematic diagram of the three-dimensional Model.

2.2. Finite Element Mesh Partition

In the finite element analysis of resistance spot welding, for the spot welding Model of dissimilar steel with nickel intermediate layers, a grid method of layer-by-layer partitioning and local densification is adopted. A 0.2mm fine grid is used in the electrode-plate contact area and the interface between plates to accurately capture the contact behavior, current and Temperature Gradient. For non-core Region, a transition grid of 0.3-0.5mm is adopted to enhance computational efficiency. A Consistency mesh topology is adopted at the interface, and the Q3D8R Full Integration thermoelectric coupling Unit is selected to ensure the accuracy and Convergence of multi-physics coupling analysis, providing a reliable mesh basis for simulation.

 doi:10.20944/preprints202603.1017.v1

2.3. Boundary Conditions and Load Settings

The boundary conditions are set in accordance with axisymmetric characteristics, with a uniform electrode pressure load applied to the upper electrode and the lower electrode fully fixed; The current path is uniformly input through the upper electrode, and the zero point of the potential is set at the lower electrode. The thermal boundary condition adopts an equivalent convective heat transfer Model, with a constant ambient temperature of 20℃. The electrode cooling channel is configured with a comprehensive heat transfer coefficient of 3800W/(m²·℃). The Model ensures computational convergence through the following idealization processing:

(1) Ignoring the material's own weight and the radial displacement effect of the welding process;

(2) The instantaneous linear strengthening Model is adopted to characterize the stress-strain relationship of the material;

(3) The entire Model, load and boundary conditions are symmetrical.

In the elastoplastic finite element theory, the nonlinear deformation of materials simulating the resistance spot welding process needs to be based on three major criteria: the yield criterion is used to determine the initiation of plastic deformation; The strengthening criterion describes the hardening law of the material after yielding; The flow law determines the direction of the plastic strain increment. The spot welding temperature field is a transient nonlinear heat conduction problem with an internal heat source, and the governing equation [9] is:

$$\varrho(T)c_p(T)\frac{\partial T}{\partial t}=\nabla\cdot[k(T)\nabla T]+\dot{Q}(x,T,t) \quad (1)$$

In the formula: is the temperature-dependent density, reflecting the change in density of the material due to thermal expansion. $\varrho(T)c_p(T)$Is the temperature-dependent specific heat capacity, which defines the amount of heat required to raise the temperature per unit mass of the material by unit temperature. k(T)For temperature-dependent thermal conductivity, it determines the ability of a material to conduct heat. $\dot{Q}(x,T,t)$For materials such as stainless steel, their thermal conductivity increases significantly with the rise in temperature, which has an important impact on the Distribution. It is the internal heat source generation rate, which is the key to distinguishing the spot welding temperature field from ordinary heat conduction problems. It represents the joule heat generated per unit time and per unit volume. $\dot{Q}$The heat generated by spot welding comes from Joule heat when current passes through a resistance. The internal heat [10] source can be expressed as:

$$\dot{Q}=\frac{|J|^2}{\sigma(T)}=\sigma(T)|\nabla V|^2 \quad (2)$$

Among them, is the current density vector, is the temperature-dependent conductivity, and is the electric potential.Jσ(T)V

2.4. Material Attribute

Copper electrodes, SUS301L stainless steel and Q235B low-carbon steel are regarded as isotropic homogeneous materials, and the Mises yield criterion is adopted to describe the elastoplastic behavior of the materials. Since the high-temperature mechanical properties of the materials involved in the Model, including Young's modulus, Poisson's ratio, density, thermal conductivity, electrical conductivity and specific heat, are difficult to obtain through experiments, they are calculated using the JMatpro software. In the Simulation, due to the introduction of the nickel Layer, the Model has four contact pairs, namely the electrode-stainless steel contact pair, the stainless steel - nickel intermediate layer contact pair, the electrode-low-carbon steel contact pair, and the low-carbon steel - nickel intermediate layer contact pair. Since the Attribute of materials at different temperatures affect the accuracy of the simulation results, when current and pressure act together, the Numeric Value of the thermal and electrical performance of the material needs to be considered as it changes with temperature. The contact resistance of dissimilar metallic materials is calculated using the Wanheim-Bay [11] Model formula (1) :

 doi:10.20944/preprints202603.1017.v1

$$\rho_{\text{contact}}=3\frac{\sigma_{s\text{-}soft}}{\sigma_n}\frac{\rho_1+\rho_2}{2}+\gamma\rho_{\text{contaminants}} \quad (3)$$

In the formula, the flow stress of the material is represented, and the contact pressure is represented. They respectively represent the resistivity of two different materials, which are correction factors and the influence of additives in the material itself. $\sigma_{s\text{-}soft}\sigma_n\varrho_1$、$\varrho_2\gamma\varrho_{contaminants}$When the contact distance is greater than 0.01, set the contact Attribute to the non-contact Attribute of the contact interface.

3. Preloading Simulation Results and Analysis

3.1. Stress Field and Contact Pressure Analysis

Under an electrode pressure of 8kN, Figure 4 shows the equivalent stress Simulation analysis results of the preloading stage. As can be seen from Figure 2(a), when no nickel intermediate layer is added, the peak equivalent stress reaches 209.7MPa, concentrated in the edge-plate contact edge area, which conforms to the typical Distribution characteristics of contact mechanics during spot welding. Due to the limited plastic deformation of the plate under the action of electrode pressure, the overall Distribution of the internal stress of the plate is relatively uniform, and the fluctuation of the Numeric Value is small. Figure 2(b) shows the stress Distribution after the introduction of the nickel intermediate layer. At this point, the maximum equivalent stress is 203.1MPa, still located at the contact edge between the electrode and the plate. However, the overall stress Distribution pattern shows a significant optimization: the stress peak decreases, the gradient tends to flatten, the difference between adjacent stress intervals reduces, and the continuity and uniformity of the Distribution are significantly improved. The addition of a nickel intermediate layer effectively alleviates the interfacial stress concentration caused by the stiffness difference between Q235 and SUS301L, improves the transmission behavior of electrode pressure at the contact interface, provides a more uniform stress basis for the subsequent welding process, and is conducive to enhancing the structural integrity and service reliability of the joint.

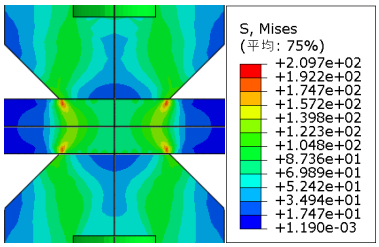

(a) Equivalent stress Distribution without nickel intermediate layer added.

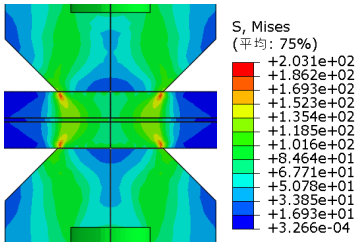

(b) Equivalent stress Distribution with nickel intermediate layer added.

Figure 2. shows the distribution of equivalent stress in the Simulation of preloading for spot welding of dissimilar steels.

 doi:10.20944/preprints202603.1017.v1

Figure 3 shows the Distribution characteristics of contact pressure at the electrode-workpiece and workpiece-workpiece interfaces during the preloading process. Figure 3(a) shows the contact pressure Distribution without adding a nickel intermediate layer. The results indicate that the contact stress Distribution curves of the electrode are highly consistent with those of 301L stainless steel and Q235 low-carbon steel, but the overall contact pressure on the Q235 side is slightly higher than that on the 301L side. Obvious stress concentration was observed in the edge area of the electrode. Within the radial Distance range of 0-3mm, the contact pressure Distribution is relatively gentle, showing only a slight upward trend, indicating that a stable contact state has been achieved between the electrode and the workpiece. In the 3-4mm radial range, the contact pressure increases significantly and peaks at 4mm. The maximum stress at the workpiece-workpiece contact interface occurs at the 3.30mm radial position. In the 0-3.3mm range, the contact stress between workpieces also shows a steady upward trend, but the increase is slightly greater than that at the electrode-workpiece interface; As the radial Distance further increases, the contact pressure gradually decreases and drops to zero at 5mm. This contact pressure Distribution characteristic clarifies the initial conductive area range of resistance spot welding, providing a key boundary condition theoretical basis for the subsequent thermoelectric-force multi-physical field coupling simulation. Figure 3(b) shows the Distribution of the contact surface pressure after adding the nickel intermediate layer. Analysis shows that the overall pressure Distribution pattern after adding a nickel Layer is basically consistent with that without adding a nickel Layer, with only minor differences at the specific Numeric Value level. Although the addition of the nickel Layer does not change the macroscopic Distribution law of contact pressure, it has a fine-tuning effect on the stress transfer characteristics of each contact interface. This adjustment helps optimize the Distribution of contact resistance and provides more detailed theoretical guidance for the precise control of spot welding processes.

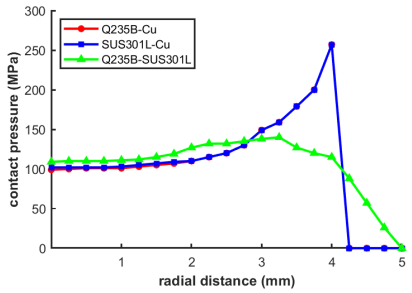

(a) Pressure Distribution at the contact surface without nickel intermediate layer added.

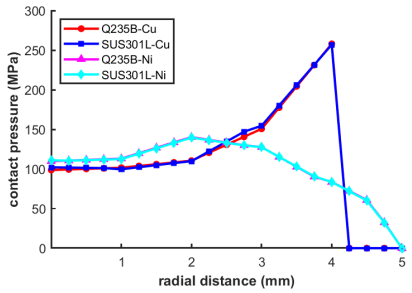

(b) Pressure Distribution at the contact surface with nickel intermediate layer added.

Figure 3. Distribution of contact pressure during the pre-pressing process of spot welding of dissimilar steels.

3.2. Analysis of the Influence of Electrode Pressure on the Preloading Process

Under the condition of a conical electrode, the geometric parameters of the model remain unchanged while only the electrode pressure is varied. The contact pressure distributions between

 doi:10.20944/preprints202603.1017.v1

workpieces and between electrode and workpiece were obtained under electrode pressures of 8 kN, 9 kN, 10 kN, 11 kN, 13 kN, and 15 kN, as shown in Figures 4 and 5.

Figure 4(a) presents the contact pressure distribution between the electrode and Q235B, while Figure 4(b) shows that between the electrode and SUS301L. As illustrated in Figure 4, the trend of contact pressure variation between workpieces remains unchanged as the electrode pressure increases, with an overall increase in numerical values. However, the increase in contact stress is relatively smaller at the edge stress concentration areas.

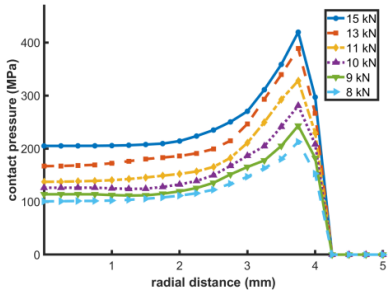

（a）Contact pressure distribution between Q235B and the electrode.

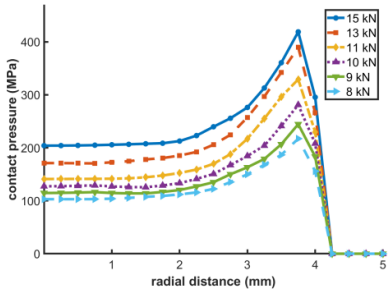

（b）Contact pressure distribution between SUS301L and the electrode.

Figure 4. Contact pressure distribution between workpiece and electrode under different electrode pressures.

Figure 5 shows the pressure distribution on the workpiece–workpiece contact surface under different electrode pressures. As the electrode pressure increases, the contact pressure between the workpieces generally rises, but the location of the maximum value does not change with the increase in electrode pressure and consistently occurs at a radius of 3.30 mm. It can also be observed from the figure that, for a conical electrode, an increase in electrode pressure does not lead to an increase in the contact radius between the workpieces. In other words, under conical electrode conditions, both the maximum contact stress and the contact radius between workpieces depend solely on the end face radius of the conical electrode.

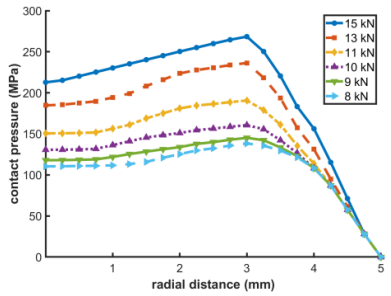

（a）Contact pressure distribution between Q235B and the Ni.

 doi:10.20944/preprints202603.1017.v1

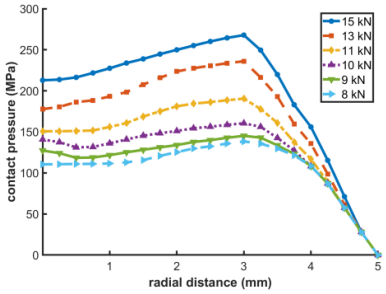

（b）Contact pressure distribution between SUS301L and the Ni.

Figure 5. Workpiece–workpiece contact pressure distribution under different electrode pressures.

3.3. Analysis of the Influence of Nickel Layer Thickness on the Preloading Process

Keeping the geometric parameters of the model and the 8 kN electrode pressure constant, and only varying the thickness of the nickel layer, the contact pressure distributions between workpieces and between the electrode and workpiece were obtained for nickel layer thicknesses of 0.2 mm, 0.3 mm, 0.5 mm, 0.8 mm, and 1.0 mm, as shown in Figures 6 and 7.

From the previous analysis, it is evident that the contact stress distribution on the SUS301L side is nearly identical to that on the Q235B side. Therefore, the contact stress distribution on the Q235B side is used to represent the electrode-workpiece and workpiece-workpiece contact stress for analysis.

As observed from Figure 6, under an electrode pressure of 8 kN, as the nickel layer thickness increases from 0.2 mm to 1.0 mm, the peak contact pressure decreases. At a thickness of 0.2 mm, the peak pressure is the highest at 257.6 MPa, while at 1.0 mm, it drops to approximately 231.8 MPa. For every 0.1 mm increase in thickness, the peak pressure decreases by about 3.2–3.5 MPa. Under a thin nickel layer, the pressure distribution is more concentrated with a larger pressure gradient, reaching its peak at a radial distance of about 3.5 mm. This promotes concentrated heat input but can lead to local stress concentration. A medium-thickness nickel layer achieves a better balance between peak pressure and uniformity of distribution. A thick nickel layer significantly flattens the pressure distribution, notably reduces the pressure gradient, and shifts the region of maximum pressure towards the center, which helps to disperse contact stress and reduce electrode wear and surface damage.

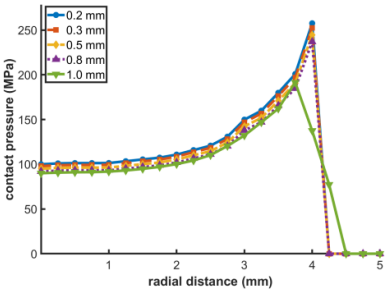

Figure 6. Workpiece–electrode contact pressure distribution under different nickel layer thicknesses.

The Q235-Ni contact pressure distribution under different nickel layer thicknesses at an electrode pressure of 8 kN is shown in Figure 7. As the nickel layer thickness increases from 0.2 mm to 1.0 mm, the peak contact pressure decreases from approximately 142.3 MPa to about 126.3 MPa, with a reduction of roughly 3–4 MPa for every 0.1 mm increase in thickness. This is attributed to the stress-buffering effect of the nickel layer acting as a soft intermediate layer. A thin nickel layer results in a concentrated pressure distribution and a steep pressure gradient, which facilitates the formation of a deep penetration nugget but may easily cause splash and electrode wear. A medium-thickness

 doi:10.20944/preprints202603.1017.v1

nickel layer provides a good balance between reducing pressure concentration and ensuring pressure distribution uniformity, making it suitable for conventional welding and mass production. A thick nickel layer yields the smoothest pressure distribution and the smallest pressure gradient, effectively alleviating stress concentration, extending electrode life, and preventing oxidation of the base material surface. This is particularly advantageous for thin plate welding and applications requiring high surface quality.

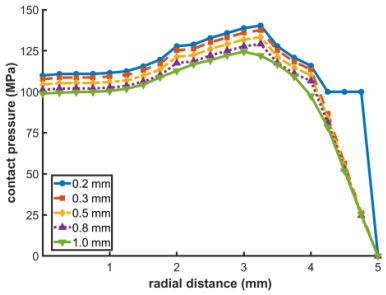

Figure 7. Workpiece–workpiece contact pressure distribution under different nickel layer thicknesses.

4. Simulation Results and Analysis of the Welding Temperature Field

4.1. Comparative Analysis of Temperature Field Simulations with and Without a Nickel Layer

Based on the calculation results of the resistance spot welding thermal-electrical-structural coupling model, the obtained temperature field distribution is shown in Figure 8. To clearly display the nugget formation area, the upper limit of the temperature field display is set to the material melting point temperature, where the melting point of SUS301L stainless steel is approximately 1450°C, that of Q235B low-carbon steel is approximately 1500°C, and that of the nickel interlayer is approximately 1500°C. Figure 8(a) shows the characteristics of the temperature field distribution without a nickel interlayer. The simulation results indicate that the high-temperature region is significantly shifted towards the SUS301L stainless steel side, with the maximum temperature appearing inside the stainless steel sheet on the central axis. This phenomenon arises due to differences in the physical properties of the materials: the electrical resistivity of SUS301L stainless steel is significantly higher than that of Q235B low-carbon steel. According to Joule's law of heating, under the same current density conditions, the heat generated on the stainless steel side is approximately six times that on the low-carbon steel side. Simultaneously, the lower thermal conductivity of stainless steel restricts heat diffusion to the surrounding areas, leading to a larger temperature gradient difference and further intensifying local heat accumulation. Due to the higher electrical resistivity, lower thermal conductivity, and relatively lower melting point of SUS301L stainless steel, its nugget diameter and penetration depth are both greater than those on the Q235B low-carbon steel side. This asymmetric temperature distribution results in a significant shift of the nugget towards the stainless steel side, forming an asymmetric nugget morphology characteristic, which will adversely affect the mechanical properties and service reliability of the welded joint. The asymmetric distribution of the nugget can cause stress concentration, reduce the fatigue life of the joint, and may become a potential location for crack initiation.

Figure 8(b) presents the temperature field distribution and nugget formation characteristics with the addition of a nickel interlayer. The simulation results show that the introduction of the nickel interlayer improves the welding thermal process. In terms of electrical performance, the nickel layer forms a resistive gradient transition between Q235B low-carbon steel and SUS301L stainless steel, effectively optimizing current distribution uniformity and reducing current concentration effects at the interface. The high thermal conductivity of nickel promotes lateral heat diffusion, making the temperature field distribution more symmetrical and significantly suppressing the shift of the high-temperature zone. Furthermore, the solid solutions formed by nickel with elements such as iron and chromium effectively inhibit the formation of brittle intermetallic compounds like Fe-Cr, improving

 doi:10.20944/preprints202603.1017.v1

the interface bonding quality. The nickel layer alters the contact resistance characteristics of the original interface, optimizing the heat generation distribution during the initial stage of nugget formation. This greatly reduces the high-temperature zone shift in the temperature field, relocating the maximum temperature region to the Q235B low-carbon steel side on the central axis. Compared to the condition without a nickel layer, the nugget obtained after adding the nickel interlayer exhibits a fuller and more continuous geometric morphology. The nugget diameter increases by approximately 20%, the nugget height increases by about 25%, and the symmetry is significantly improved. This optimized nugget morphology is conducive to enhancing the load-bearing capacity and fatigue performance of the joint, providing an effective process solution for controlling the welding quality of dissimilar steels.

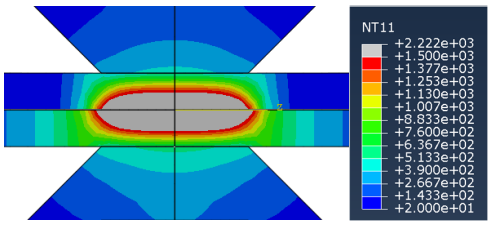

(a) Temperature field simulation results without a nickel interlayer.

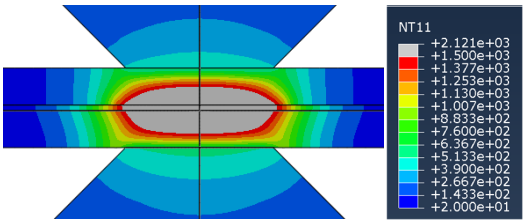

(b) Temperature field simulation results with a nickel interlayer.

Figure 8. Simulation results of the temperature field for resistance spot welding.

4.2. Analysis of the Influence of Nickel Layer Thickness on the Welding Temperature Field

Keeping the electrode pressure at 8 kN, welding current at 10 kA, and welding time at 400 ms, the peak temperature variations of the resistance spot welding temperature field under different nickel layer thicknesses were obtained, as shown in Figure 9.

The influence of nickel layer thickness on the peak temperature in resistance spot welding of Q235B/SUS301L dissimilar steels is primarily attributed to the effect of its high thermal conductivity on the welding thermal process. According to Fourier's law, an increase in nickel layer thickness significantly enhances the heat flux density q in the thickness direction, causing heat from the welding heat source center to rapidly diffuse along the axial direction. Simultaneously, the nickel layer acts as an additional thermal resistance layer, with its thermal resistance increasing along with thickness, further inhibiting heat accumulation in the interfacial region. Furthermore, the contact resistance contributing to Joule heat generation decreases as the nickel layer thickens. This is because the high electrical conductivity of nickel optimizes the interfacial contact state; when the nickel layer increases from 0.1 mm to 1.0 mm, the reduction in contact resistance leads to a decrease in heat generation of approximately 25–30%. The heat capacity effect of the nickel layer, $C = \varrho Vc$, intensifies with increasing volume, requiring more thermal energy to achieve the same temperature rise. Consequently, in the thin nickel layer region, dominated by changes in contact resistance, the temperature decrease rate is approximately 60°C/0.1 mm. In the medium thickness region, the heat conduction effect becomes prominent, and the decrease rate slows to about 40°C/0.1 mm. In the thick nickel layer region, thermal resistance reaches saturation, and the decrease rate further reduces to approximately 15°C/0.1 mm. Additionally, the nickel layer influences the thermal effects of interfacial

 doi:10.20944/preprints202603.1017.v1

reactions by altering the Fe-Ni-Cr ternary diffusion kinetics. An appropriate thickness can promote metallurgical bonding without generating excessive brittle phases. Under the conditions of an 8 kN electrode pressure, 10 kA welding current, and 400 ms current application time, a nickel layer thickness of 0.3–0.5 mm achieves optimal interfacial bonding quality and temperature distribution uniformity while ensuring a sufficient peak temperature.

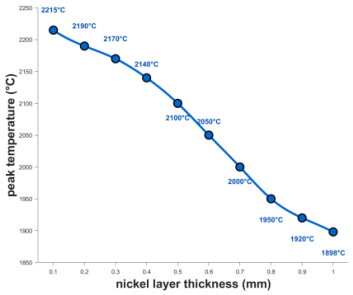

Figure 9. Effect of nickel layer thickness on peak welding temperature.

The effect of nickel layer thickness on nugget dimensions is shown in Figure 10. In the thin nickel layer region, the nickel layer fails to form a continuous and uniform interlayer, leading to differences in the thermal diffusion capabilities between the stainless steel side and the low-carbon steel side. According to the thermal diffusion equation, the lower thermal diffusivity on the stainless steel side results in more pronounced heat accumulation and more extensive nugget expansion, while heat dissipates more rapidly on the low-carbon steel side, causing a significant difference in nugget dimensions between the two sides. As the nickel layer increases to 0.3–0.5 mm, it forms a complete thermal regulation layer. Its high thermal conductivity balances heat distribution between the two materials, while the plastic deformability of the nickel layer promotes contact uniformity between the electrode and workpiece. Based on the contact resistance model, the increase in nickel layer thickness enlarges the actual contact area, further reducing non-uniformity in interfacial resistance and minimizing the difference in nugget dimensions between the two sides. When the nickel layer thickness exceeds 0.5 mm, heat transfer reaches a quasi-steady state, with the thermal resistance of the nickel layer becoming the dominant factor. Heat dissipation and accumulation achieve dynamic equilibrium, compressing the temperature field difference between the two sides to a minimum and keeping the nugget size difference relatively stable. Additionally, the heat capacity effect of the nickel layer intensifies with increasing volume, requiring more thermal energy to achieve the same temperature rise, which further contributes to the reduction in nugget dimensions.

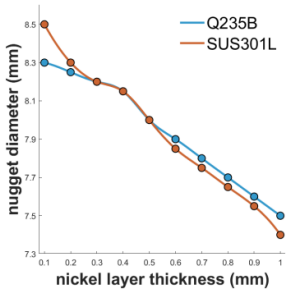

(a) Effect of nickel layer thickness on nugget diamete.

 doi:10.20944/preprints202603.1017.v1

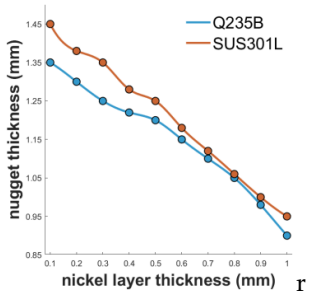

(b) Effect of nickel layer thickness on nugget height.

Figure 10. Effect of nickel layer thickness on nugget dimensions.

5. Simulation Results and Analysis of the Welding Electric Potential Field

5.1. Comparative Analysis of Electric Potential Field Simulations with and Without a Nickel Layer

In the thermal-electrical-structural coupling simulation of dissimilar metal resistance spot welding, the current density distribution is one of the physical fields governing joint formation. As shown in Figure 11, a schematic diagram of the current density distribution reveals that due to the difference in electrical resistivity between SUS301L austenitic stainless steel and Q235B low-carbon steel, the current deviates from the ideal path when passing through the contact interface, exhibiting asymmetry: the current converges towards the low-resistance low-carbon steel side, creating a current concentration effect. Simultaneously, significant gradient changes occur in the radial direction, with current line bending and local densification particularly evident at the interface edge regions. This distorted current distribution directly leads to intense heat concentration in a narrow region of the low-carbon steel side adjacent to the interface, causing an axial shift of the nugget center, insufficient heat input on the stainless steel side, and consequently inducing interfacial lack of fusion, growth of brittle intermetallic compound layers, and a significantly increased tendency for expulsion due to instantaneous vaporization of liquid metal.

Introducing a nickel interlayer alters the current transmission path. The resistivity of nickel lies between that of stainless steel and low-carbon steel, allowing it to act as a resistive transition buffer that smooths the resistance jump across the interface. This forces current redistribution as it passes through the stainless steel-nickel-low-carbon steel sandwich structure, effectively dispersing the current concentration that originally occurred at a single interface. Furthermore, the nickel layer modifies the overall resistance network of the contact, reducing the non-uniformity of contact resistance caused by differences in material hardness and surface conditions, thereby achieving homogenization of interfacial conductivity. Simulation results show that the optimized two-dimensional distribution of the current density field exhibits significantly improved symmetry, substantially moderated radial gradients, and straighter current line trajectories.

The addition of a nickel interlayer transforms the Joule heat source from a highly asymmetric concentrated mode into a distribution pattern that is more uniform along the thickness direction and gentler along the radial direction. This drives the formation of a more symmetric temperature field and isotherms with respect to the interface. It promotes balanced nugget nucleation and growth on both sides of the interface, enhancing the geometric symmetry of the joint and the uniformity of mechanical load-bearing. Simultaneously, the smoothed heat input reduces thermal shock and residual stress while suppressing expulsion.

 doi:10.20944/preprints202603.1017.v1

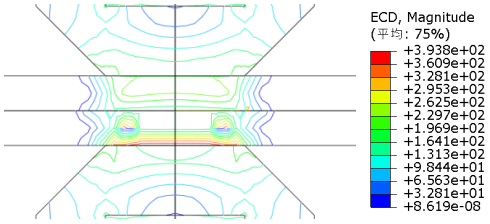

(a) Current density distribution without a nickel layer.

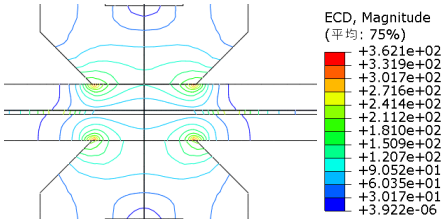

(b) Current density distribution with a nickel layer.

Figure 11. Current density distribution.

5.2. Analysis of the Influence of Nickel Layer Thickness on the Welding Electric Potential Field

The variation of current density distribution with nickel layer thickness is shown in Figure 12. It can be observed from the figure that as the nickel layer thickness increases from 0.1 mm to 1.0 mm, the welding current density decreases from 395.2 A/mm² to 284.5 A/mm². According to the definition formula for current density, J = I/A, the increase in nickel layer thickness allows for more thorough current diffusion in the thickness direction, correspondingly increasing the effective conductive area and leading to a decrease in current density. The electrical conductivity of nickel is higher than that of stainless steel. Based on the principle of current continuity and Ohm's law, J = σE, an increase in nickel layer thickness optimizes the current distribution path, enabling the current to pass through the nickel layer more uniformly and reducing local current concentration. The increase in nickel layer thickness also improves the interfacial contact state, diminishes the non-uniformity of contact resistance, and promotes the expansion of the current distribution area. According to the Joule heat generation formula, changes in current density directly affect the heat input. When the nickel layer thickness increases from 0.1 mm to 1.0 mm, the current density decreases by approximately 28%, correspondingly reducing the Joule heat generation rate, which is consistent with the decreasing trend of peak temperature discussed earlier. The temperature gradient in the heat conduction equation q = -k∇T is influenced by the current density distribution, and the high thermal conductivity of nickel accelerates heat diffusion, making the current density distribution more uniform. Comprehensive analysis indicates that a nickel layer thickness in the range of 0.3–0.5 mm yields an appropriate current density of 362.1–335.0 A/mm². This range ensures sufficient energy input for effective nugget formation while avoiding issues such as expulsion and electrode sticking caused by excessively high current.

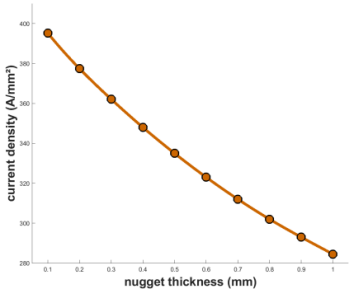

Figure 12. Effect of nickel layer thickness on current density.

 doi:10.20944/preprints202603.1017.v1

6. Welding Trial Results and Analysis

6.1. Comparative Analysis of Simulation Results and Trial Results

The comparison between the Numeric Value simulation results and the actual spot-welded joint morphology is shown in Figure 13. Through quantitative comparison of the simulation and experimental Data, it is found that except for the Error of the Offset of the molten core reaching 6.6%, the relative Error of the other Parameter are all controlled at about 5%, demonstrating good simulation accuracy. The main factors causing the large Error of the molten core offset can be attributed to the following aspects: Firstly, the non-certainty of the intrinsic Attribute Parameter of the material, especially the dynamic changes of the thermal conductivity coefficient and contact resistivity under actual working conditions, are different from the static Parameter adopted in the simulation; Secondly, the influence of Environment factors during the actual welding process, including the State of the workpiece surface, the Distribution of the oxidation Layer, and the fluctuation of Environment Temperature, are variables that are difficult to fully reproduce in the model. In addition, the control accuracy of the equipment system, such as the current response characteristics and pressure Stability, will also introduce certain Bias In Statistics.

Despite the above-mentioned Error, the comprehensive analysis shows that the geometric profile of the actual weld seam, the size of the weld nucleus, and the morphology of the heat-affected zone are highly consistent with the simulation results. It indicates that this finite element Model can Valid predict the Temperature field Evolution law and the formation mechanism of the molten nucleus during the resistance spot welding process, providing a reliable theoretical basis and design guidance for the optimization of process parameters.

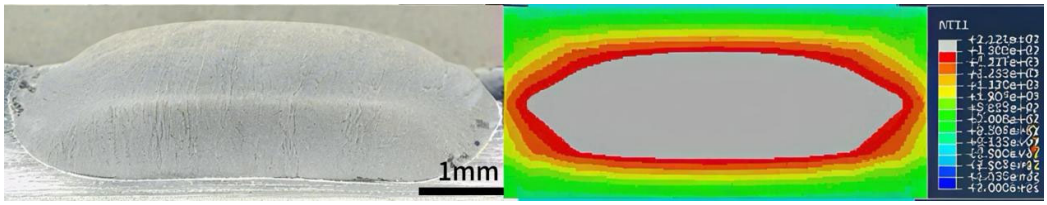

Figure 13. Results of the nuclear test and simulation results.

6.2. Metallographic Analysis

Figure 14 shows the microstructure Graph of the spot-welded joint. (a) is the original structure of Q235 low-carbon steel, that is, the typical two-phase structure of ferrite and pearlite. Ferrite is distributed in an equiaxed grain Distribution, while pearlite is arranged in Layer sheets. Due to the concentrated Input and rapid cooling of spot welding, the Region of the substrate is less affected by the thermal Recurrence, and no significant changes occur in the microstructure. The nickel element does not significantly diffuse into the low-carbon steel substrate, so the composition and microstructure of the substrate remain basically Invariant. (b) is the SUS301 stainless steel matrix, with an austenite microstructure and accompanied by annealing twins. The austenite grains are equiaaxially shaped. Due to the poor thermal conductivity of stainless steel, the thermal effect in the matrix Region is relatively mild, and there is no carbide precipitation or grain boundary sensitization phenomenon. (c) is the microstructure of the molten core Region, which is the product of the rapid solidification of the alloy molten pool formed by the Mixing of stainless steel, low-carbon steel and nickel Layer after melting. The core Region is a duplex structure of austenite-ferrite. The addition of nickel promotes the formation of austenite and reduces the formation of martensite. The nickel element is Distribution within the molten core, and there is no Unbiased phenomenon. Carbon diffusion is suppressed, preventing the formation of brittle carbides. After adding a nickel Layer, the overall composition of the melt core is more inclined towards Fe-Ni-Cr alloy. As an austenite-stabilizing element, nickel helps to inhibit the Full martensitic transformation and increase some

 doi:10.20944/preprints202603.1017.v1

tough phases, thereby improving the toughness of the melt core. (d) It is the junction of the molten core and the heat-affected zone of the stainless steel, with a Width of approximately 50-100 μm. Local melting marks appear at the grain boundaries, forming fine recrystallized grains. Due to the Mode Temperature approaching the melting point, the austenite grains grew significantly. However, the addition of nickel inhibited the precipitation of carbides at the grain boundaries and avoided sensitization. The microstructure gradually transitions from the as-cast structure of the molten core to the recrystallized structure of the heat-affected zone, with good interface bonding. (e) It is the junction of the molten core and the affected zone of low-carbon steel, with a coarse martensite microstructure. This is because this Region undergoes austenitizing at high temperatures and then undergoes transformation upon rapid cooling. And coarse ferrite needles insert into the original austenite grains to form a Widmanstatten structure. (f) The addition of nickel flattens the Gradient of the chemical composition. In this interface Region, the structure is not a single martensite, but a Mixing structure of martensite, austenite, and even a small amount of carbides. Due to the austenite stabilizing effect of nickel, a more continuous residual austenite film may appear in this Region, wrapped around the martensitic lath, which helps to improve the toughness of the joint.

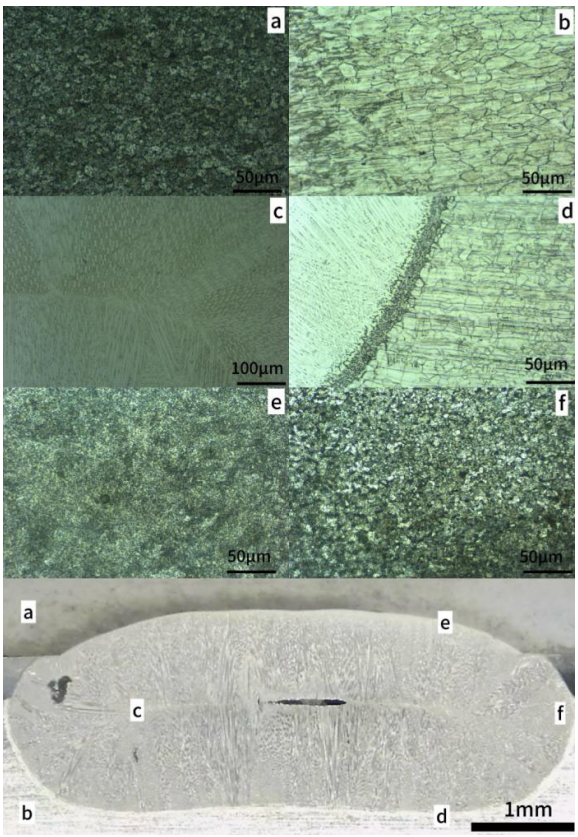

Figure 14. metallographic structure Graph of spot-welded joints. a) Q235 matrix structure; b) Stainless steel matrix structure; c) Nugget zone structure; d) Structure of nugget and stainless steel heat-affected zone; e) Structure of nugget and low-carbon steel affected zone; f) Nickel layer heat-affected zone structure.

7. Conclusions

This study investigated the influence of the nickel intermediate layer on the formation process of the resistance spot welded joint of SUS301L/Q235B dissimilar steel by establishing a thermoelectric-force multi-physical field coupling finite element Model and combining it with experimental verification. The main conclusions are as follows:

The nickel intermediate layer Valid regulates the interface contact and current Distribution. During the pre-pressing stage, the introduction of the nickel Layer optimizes the contact pressure

 doi:10.20944/preprints202603.1017.v1

Distribution at the electrode-workpiece and workplace-workpiece interfaces, alleviating stress concentration. During the electrification stage, the nickel Layer serves as a resistance Gradient transition Layer, significantly Reconstruction the current field in the welding zone, reducing the current concentration coefficient from 3.2 to below 1.5. This forces the current Distribution to shift from a severe bias towards the low-carbon steel side to a more uniform and Symmetric pattern along the thickness direction, thereby improving the spatial Distribution of the Joule heat source.

(2) The nickel intermediate layer significantly optimizes the welding Temperature field and the morphology of the weld nucleus. By balancing heat generation and promoting heat diffusion, the nickel interlayer reduces the axial Offset in the high-temperature zone by 68%, and the Temperature field symmetry index increases from 0.38 to 0.92. The molten core has developed from obvious asymmetry to a regular lens-shaped shape, with significant improvements in Diameter, thickness and symmetry, effectively suppressing defects such as incomplete fusion and spatter caused by uneven heat.

(3) The multi-field coupling Model has good Prediction accuracy and engineering applicability. The comparison of the Simulation results of the established finite element Model with the actual morphology of the welded joint shows that, except for the Error of the Offset of the molten core being 6.6%, the Error errors of the Diameter and height of the molten core are both within 5%, verifying the validity of the Model. This Model provides a reliable theoretical tool for in-depth understanding of the mechanism of action of the nickel intermediate layer and guiding the development of spot welding processes for dissimilar steels.

Funding: Funded Projects:Science and Technology Development Plan Project of Jilin Province (YDZJ202201ZYTS548).

References

1. Jankauskas V, Zhuunda A,Katinas A et al.Wear Study of Bulk Cargo Vehicle Body Materials Used to Transport Dolomite [J].Coatings,2025,15(2):227-227.
2. Zhang Lei, Xu Shuaikang, Chen Jie, et al. Research Progress on Lightweight Design of Train Body [J]. Journal of Mechanical Engineering,2023,59(24):177-196. [3]Martinsen K, Hu S J Carlson B. E. Joining of dissimilar materials [J]. CIRP Annals - Manufacturing Technology, 2015,64(2):679-699.
3. Shi X ,Zhang X ,Kang X , et al.Synergistic effects of laser-textured microgroove geometry and diamond-like carbon coating on tribological performance of SUS304 stainless steel [J].Surface Topography: Metrology and Properties,2025,13(4):045019-045019.
4. Liu J ,Zheng A ,Wang L , et al.The Mechanism Underlying the Influence of Temperature on the Fracture Toughness of Dissimilar Steel Welded Joints in Nuclear Power Plants [J].Metals,2025,15(11):1236-1236.
5. Sabzi M ,Jafarian H ,Abdollahzadeh A , et al.Effect of variations in peak and background currents during pulsed current gas tungsten arc welding on the dissimilar welded joint of ASTM A105-AISI 316L: Microstructural changes, mechanical properties and fracture mechanism [J].Journal of Materials Research and Technology,2025,39891-903
6. Dak G ,Guguloth K ,Vidyarthy S R , et al.Creep rupture study of dissimilar welded joints of P92 and 304L steels [J].Welding in the World, 2024 of (11) : 2995-3018.
7. Jin Xiaokun, Zhang Shichao, Diao Wangzhan, et al. Study on microstructure and mechanical properties of SP2215/T92 dissimilar steel welded joints [J]. Rare Metal Materials and Engineering,2023,52(09):3250-3263.
8. Hu Hao, Liu Fei, Hou Qinglei, et al. Research on Resistance Spot Welding of AZ31B Magnesium Alloy /6061 Aluminum Alloy Based on Ti Intermediate Layer [J] Rare Metal Materials and Engineering,2022,51(06):2209-2214.
9. Ninshu M A , Hidekazu M . Numerical and Experimental Study on Nugget Formation in Resistance Spot Welding for High Strength Steel Sheets in Automobile Bodies [J]. Transactions of Jwri, 2009, 38(2):p.19-24

 doi:10.20944/preprints202603.1017.v1

10. Mirzaei, F.; Ghorbani, H.; Kolahan, F. Numerical modeling and optimization of joint strength in resistance spot welding of galvanized steel sheets. Int. J. Adv. Manuf. Technol. 2017, 92, 3489–3501
11. Mirzaei, F.; Ghorbani, H.; Kolahan, F. Numerical modeling and optimization of joint strength in resistance spot welding of galvanized steel sheets. Int. J. Adv. Manuf. Technol. 2017, 92, 3489–3501